Research Article | Vol. 33, No. 13 / 30 Jun 2025 / Optics Express 28071
Optics EXPRESS

# Multi-millijoule hollow-core fiber compression of short-wave infrared pulses to a single cycle

JOHANNES BLÖCHL,[1,2] MAXIMILIAN F. KUTHE,[1,2] HARTMUT SCHRÖDER,[2] ABDALLAH M. AZZEER,[3] THOMAS NUBBEMEYER,[1,2] AND MATTHIAS F. KLING[1,2,4,5,*]

[1]Department of Physics, Ludwig-Maximilians-Universität Munich, D-85748 Garching, Germany
[2]Max Planck Institute of Quantum Optics, D-85748 Garching, Germany
[3]Attosecond Science Laboratory, Physics and Astronomy Department, King Saud University, Riyadh 11451, Saudi Arabia
[4]SLAC National Accelerator Laboratory, Menlo Park, CA 94025, USA
[5]Applied Physics Department, Stanford University, Stanford, CA 94305, USA
*kling@stanford.edu

**Abstract:** Approaches for efficient pulse compression can enable dramatic increases in the available peak power, as well as enable the generation of isolated attosecond X-ray pulses. Achieving high compression ratios for longer wavelength drivers has, however, been challenging. We present the compression of few-cycle 2.1 µm central wavelength short-wave infrared laser pulses to 6.9 fs with 2.35 mJ pulse energy at a 10 kHz repetition rate. Electric field resolved measurements reveal a single cycle light field oscillation. With a carrier-envelope-phase stability of 131 mrad and average power fluctuations below 1 %, the system constitutes an excellent light source for strong-field experiments and attosecond physics.



## 1. Introduction

Advances in laser development propel modern science and technology [1–3]. In particular the combination of a high peak power at infrared wavelengths and increasingly shorter laser pulse envelopes paves the way for strong-field experiments even in the relativistic region [4], or for attosecond science reaching the X-ray range [5]. In pursuit of the generation of such short laser pulses, frequency broadening in hollow-core fibers (HCFs) has emerged as the gold standard [6–8]. Whereas the generation of additional frequency components in the laser spectrum was initially decoupled from subsequent compression (e.g. via chirped mirrors [9,10]), novel approaches tune the fiber parameters for self-compression [11,12], soliton propagation [13], or the generation of dispersive waves in the ultraviolet [14–16] or mid-infrared [17]. In particular, the interplay between the dispersion introduced by the gas, the non-linear interaction and the dispersion of the waveguide allows self-compressing schemes, where those contributions counteract each other [11,14]. This development is profiting from the concept of stretched hollow-core fibers that can be extended to several meters in length [18]. Besides that, hollow-core photonic crystal fibers have successfully been employed for the generation of super broadband continua [7,15,19,20]. The maximum achievable peak power is limited by the damage threshold, but peak powers up to the gigawatt range have been demonstrated [21–23].

For the waveguide dispersion to become significant, smaller fiber core radii $r$ are preferable due to the $\propto r^{-2}$ scaling of the waveguide dispersion [14], even though they are prone to losses [14]. Typically, additional limitations are set by self-focusing and ionization [24–26] that prevent the usage of arbitrarily small fibers for high power lasers. For the achievement of self-compression in fibers, infrared laser sources are especially appealing due the increasing waveguide dispersion with longer wavelength [12,14,27,28]. A combination of state of the art short-wave infrared

#564364 https://doi.org/10.1364/OE.564364
Journal © 2025 Received 4 Apr 2025; revised 28 May 2025; accepted 28 May 2025; published 24 Jun 2025

Optics EXPRESS

(SWIR) laser systems with self-compressing spectral broadening systems thus promises the generation of very high-peak powers due to the aforementioned scaling laws.

In this article, we demonstrate a self-compressing broadening scheme for a multi-millijoule SWIR laser source. Driven by a 2.1 $\mu$m optical parametric chirped pulse amplifier [29], we generate a multi-octave spanning spectrum that self-compresses to 6.9 fs, which marks the single-cycle regime. With 2.35 mJ pulse energy at 10 kHz repetition rate and 138 mrad rms carrier-envelope-phase (CEP) fluctuations, the presented light source constitutes an excellent driver for high-harmonic generation with amplitude gating [5] or for the generation of tesla scale magnetic impulses [30,31]. To the best of our knowledge, our system constitutes the highest peak-power, multi-millijoule, multi-kilohertz, single-cycle and CEP stable SWIR laser system, see Fig. 1 for a comparison of related systems from the recent literature. Since high laser peak powers can be achieved by either increasing the pulse energy or by compressing the pulses and thus confining the energy in a shorter interval of time, it is necessary to compare the peak power of a system to the pulse duration to distinguish the technical approach. In Fig. 1, we compare the performance for SWIR systems with a repetition rate in the range from 1 kHz to 100 kHz. We estimate the peak power of the related literature systems, unless specified, by assuming that 90 % of the pulse energy is confined in the main peak of a sech$^2$ pulse, which transfers to a conversion via $P_{\mathrm{peak}} = 0.88 \cdot \frac{0.9E_{\mathrm{pulse}}}{\tau_{\mathrm{FWHM}}}$, where $\tau_{\mathrm{FWHM}}$ is the full-width at half-maximum pulse duration. This assumption might overestimate the performance of some systems. The assumption of a sech$^2$ pulse shape is arbitrary, but the difference to other commonly used models, such as Gaussian pulses, is below 7 %. For our system, however, we use the exact value for the peak power extracted from the field-resolved data presented below.

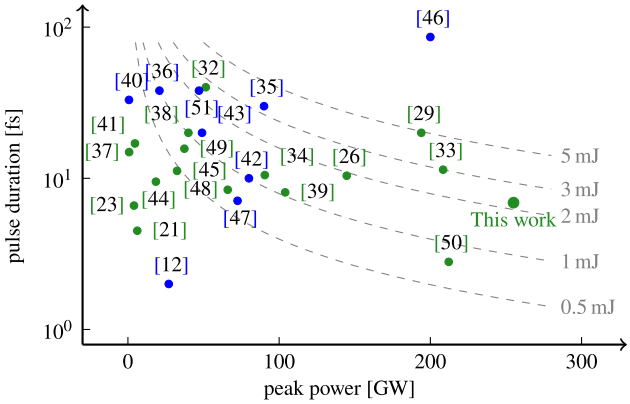


**Fig. 1.** Overview of state of the art laser systems in the SWIR region [12,21,23,26,29,32–51]. Green: CEP stable systems, blue: not CEP stable. The dashed lines indicate the pulse energy according to our conversion law. For systems with a peak power different than that, however, they do not apply.

## 2. Experimental approach

The laser front-end is a CEP-stable optical parametric chirped pulse amplifier reported elsewhere [29]. It is operated at 4.5 mJ pulse energy corresponding to 45 W average power at a central wavelength of $\lambda_0 = 2.1$ $\mu$m with a pulse duration of 23 fs as confirmed via frequency-resolved optical-gating [52,53]. A portion of 3.75 mJ is focused with an $R = -2500$ mm radius of curvature spherical mirror into a 700 $\mu$m core-diameter hollow fiber, see Fig. 2. The beam angle and position is actively stabilized (Aligna TEM Messtechnik GmbH) and the set point is used for alignment of the beam through the fiber. The latter is stretched between two internally developed

Optics EXPRESS

and adjustable fiber mounts and has a length of 2.4 m. One mount (depending on the desired setup) is placed on a movable stage for adjusting the tension of the fiber by a spring. That mechanism guarantees that a thermal expansion of the fiber during operation is compensated. We find that the expansion is typically less than 0.5 millimeters in our setup, therefore, the movable part can also be placed at the entrance since the maximum travel distance is smaller than the Rayleigh length. The fiber is filled with 700 mbar of Neon at a static pressure. After the exit, a 1 mm $CaF_2$ window allows for evacuating the subsequent beam path or for coupling the beam out for experiments at ambient air. After re-collimation, the beam is sent to a TIPTOE setup as well as to a $2f$-$3f$ interferometer for CEP control and measurement, besides other means of diagnostics. The input and output spectra are amplitude calibrated with a calibration lamp and shown in Fig. 2. The input spectrum is taken with an OceanOptics NIRQuest-512 (0.9 to 2.5 $\mu$m), whereas the output spectrum is taken with three devices, OceanOptics HDX (Si) and NIRQuest-512 (0.8 $\mu$m-1.6 $\mu$m, InGaAs), as well as Spectral Products SM301-EX (PbSe).

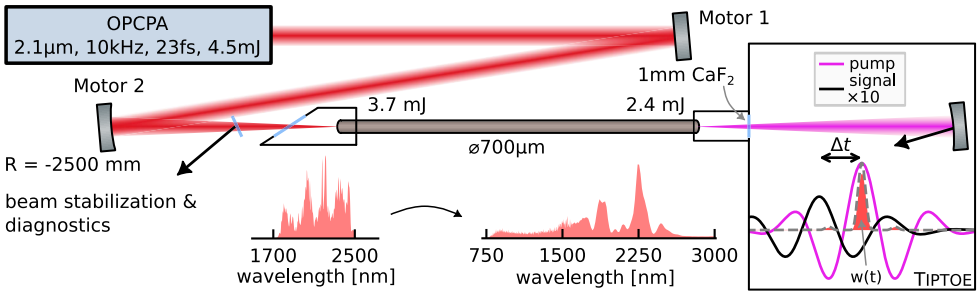


**Fig. 2.** Fiber broadening with the 2.1 $\mu$m OPCPA laser. The black boxes indicate vacuum chambers that can be pumped and filled individually. The distances in the figure are not to scale. The spectra shown have a linear scale for the intensity amplitude. The TIPTOE box also includes other means of diagnostics, such as a $2f-3f$ interferometer or a powermeter.

We characterize the output of our system with the tunneling ionization with a perturbation for the time-domain observation of an electric field (TIPTOE) [54] which has proven its reliability in measuring laser pulses from the ultraviolet, visible or infrared regime [55], via ionization in gases [54], solids [56] or micro- and nano-structures [57–59]. As a first experimental application of the multi-octave spanning spectrum of our laser pulses, we investigate CEP effects in the spectral response of TIPTOE. In particular, we exploit the CEP dependent sensitivity of TIPTOE at harmonics of the central frequency [56,57,59] for an intrinsic calibration of the CEP owing to our broad spectrum.

The main principle of TIPTOE, as presented in Ref. [54] and outlined in the corresponding box in Fig. 2, is based on a strong pump beam, $E_{\mathrm{Pump}}$, that generates an ion yield $Q$ in a gas by sub-cycle field ionization during its strongest optical half-cycle. This ion yield is linearly perturbed by a second weak beam, $E_{\mathrm{Signal}}$, delayed by a time $\Delta t$, which modulates the ion yield according to the interference of both beams during the sub-cycle ionization gate. The ion yield can be estimated via the ionization rate $w(t)$, see Supplement 1. For those measurements, we employ a Mach-Zehnder-type interferometer that contains perforated mirrors as dispersion free beam-splitters. The transmitted part of the beam ($E_{\mathrm{Signal}}$) contains a piezo-driven retro reflector and an optical chopper enabling lock-in detection of the ion yield modulation. For delay control, the interference pattern of a co-propagating frequency-stabilized HeNe laser is detected with a camera and stabilized by feedback to the piezo driver. The intensity ratio in the focus is $I_{\mathrm{Signal}}/I_{\mathrm{Pump}} \approx 3 \times 10^{-4}$, where Pump refers to the reflected beam in the interferometer. The perturbing field strength is only 1.7% of that of the pump.

Optics EXPRESS

## 3. Power and CEP stability

To uncover the performance of our fiber broadening system, we investigate the power and CEP stability as well as the beam profile. We achieved a transmitted power of 23.5 W that is stable within a standard deviation of 0.226 W, corresponding to 0.96 %, as measured over a time interval of more than 50 minutes (Fig. 3(a)). The corresponding transmission is 63 %. The expected value we found from simulation with the code from Ref. [60] is around 90 % and deviates from our value due to in-coupling losses in our setup. The beam-profile of the fiber output in the focus of a $f$ = 400 mm spherical mirror measured with a micro-bolometer camera is shown in Fig. 3(b), together with the profile of the collimated beam (part c) and d)). In Fig. 3(c), we added a 1 $\mu$m longpass filter to show that the short wavelengths are closer on axis when compared to the full beam-profile in d). The spatial distribution of the spectral components has influence on the field-measurements, see discussion in the Supplement 1.

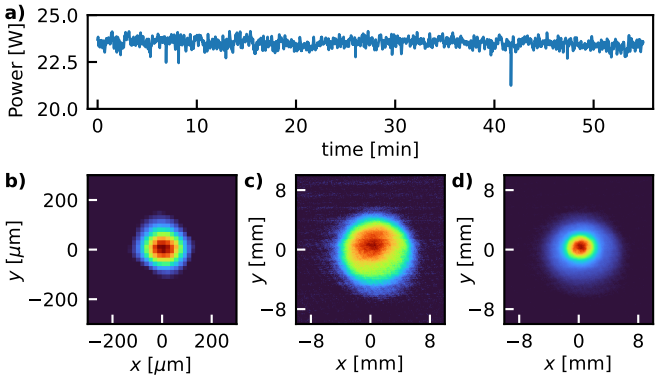


**Fig. 3.** **a)** Power stability measurement yielding 23.5 W average power at the fiber exit with a standard deviation of 226 mW, which is 0.96 %. **b)** Focus of the fiber output with a $f$ = 40 cm spherical mirror on a Rigi Microbolometer camera. **c)** Collimated beamprofile on a Pyrocam IV, with 1 $\mu$m longpass filter and without (**d**)).

We confirmed the CEP stability of the fiber output by measuring $2f$-$3f$ interference fringes in an out-of-loop measurement, while stabilizing it with an in-loop PID control. Here, the $2f$ spectral components generated via frequency doubling in $\beta$-barium borate overlap conveniently in the range of silicon detector with the third harmonic that is generated in the fiber. Thus, we could exploit readily available silicon based spectrometers for detection. The extracted relative CEP from the interference fringes is detected over an extended period of time as shown in Fig. 4(a) and its fluctuations amount to a standard deviation of 138.2 mrad. Here, we acquire a spectrogram every 64 ms, thus fast CEP modulations are not resolved. When measuring the single-shot CEP stability of our system, we find a value of 381.1 mrad, see Fig. 4(b). There, we use our triggered spectrometer (Avantes Avaspec ULS-4096CL-EVO-UA-10) to acquire a spectrum for a single laser shot. We set the integration time to 90 µs, shorter than the 100 µs time between two consecutive laser pulses to ensure only a single pulse is detected. However, we cannot measure the CEP for every consecutive shot due to a dead time of the device after an acquisition of 698 $\mu$s [61]. Thus, we expect that at least 7 pulses are skipped between each frame in the single-shot data. Nevertheless, we believe that the single-shot measurement confirms that the CEP stability is maintained from a near shot-to-shot basis to a one-hour-scale. To the best of our knowledge, this is the highest CEP stability of a multi-kilohertz, multi-millijoule, single-cycle 2 $\mu$m based system.

Optics EXPRESS

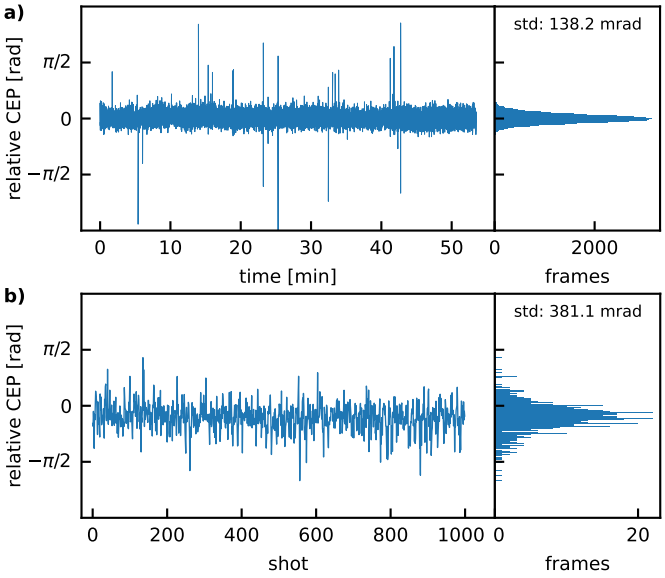


**Fig. 4.** **a)** The extracted phase of the $2f$-$3f$-fringes after the fiber shows a standard deviation of 138 mrad over a time of more than 50 minutes. **b)** Single-shot CEP data exhibiting a standard deviation of 381.1 mrad for 1000 shots.

## 4. Characterization of the time-domain electric field

The measurement of the pulse shape and duration is particularly challenging for super broadband spectra. For multi-octave spanning spectra, the measurement of the electric field of the laser pulse is the appropriate approach. Therefore, we perform TIPTOE-measurements [54] for the characterization of our system. The measured TIPTOE waveforms are shown in Fig. 5(a) for a relative CEP of the input pulses of 1.5 rad and 3.1 rad as stabilized with the $2f$-$3f$ interferometer. The full-width at half-maximum (FWHM) pulse duration of the intensity envelope is 6.9 fs, which is even shorter than the cycle-time associated with the central wavelength of the input of $\approx$ 7 fs. This value corresponds to a peak power of 0.26 TW. For the time-domain electric fields, we apply a Tukey-window in Fourier space to select the frequency components between 0.03 and 0.5 PHz. To sample such short pulses, we place an additional 0.3 mm fused silica plate before the TIPTOE setup when the chamber is pumped down to a millibar regime, and 0.6 mm fused silica if at room pressure. We do not observe a significant elongation of the main pulse in the TIPTOE measurement depending on the gas pressure when compensating for the dispersion, however, we do see the formation of side pulses due to the higher amount of of dispersive media being present in the beam path. Additionally, we observe an increasing signal-to-noise ratio when reducing the pressure. We believe that this is an effect of the bias voltage (10.6 V) being more appropriate at lower pressures, similarly to Ref. [54], where a higher bias voltage was used in the ambient air measurements. The data shown in Fig. 5(a) is taken at a pressure of 10 mbar.

The CEP is shifted for both pump and signal beam synchronously. This simultaneous shift can, however, not be measured with TIPTOE since it is only sensitive to the CEP difference between both beams (c.f. Refs. [54,55,57,59] and Supplement 1). Thus, the CEP of the measured waveform is not supposed to change with the CEP of the laser pulses and only represents the actual electric field if the CEP of the pump beam is 0. Consequently, a calibration of the CEP of the pump is necessary which was done previously using a second harmonic field [54]. Profiting from the multi-octave bandwidth of our laser system, we can intrinsically calibrate the CEP by observing the resolved spectral amplitudes in the $2f$ region of the central frequency $f$, in

Optics EXPRESS

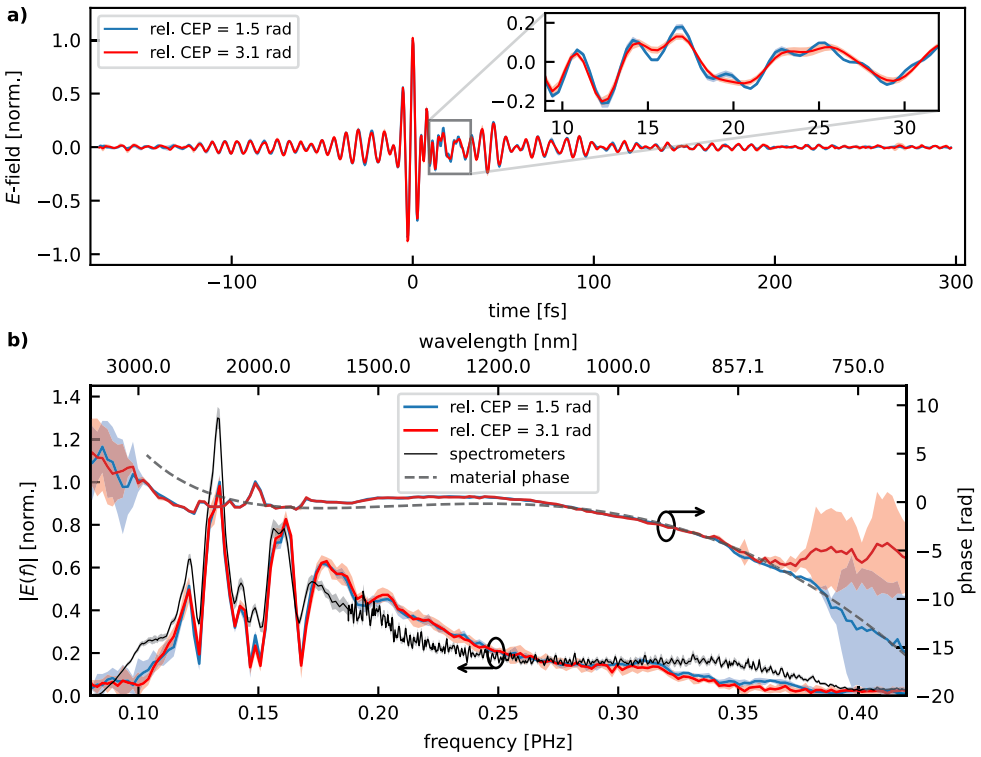


**Fig. 5.** **a)** Time-domain electric field (blue) and measured waveform for a different CEP (red). **b)** spectral field amplitudes corresponding to the waveforms in a). Effects of the CEP of the laserpulses are visible between 0.3 and 0.38 PHz. Spectral amplitudes of the fiber output measured with spectrometers (black line). The arrows indicate the corresponding axis.

particular from 0.3 to 0.38 PHz. There, the resolved spectral amplitudes are enhanced for a CEP of the pump of 0. The results of a CEP scan and the observation of the expected modulations in the 2*f* region, see supplement, identify the relative CEP of 1.5 rad with a pump beam CEP of 0. Thus, the waveform shown in that case represents the electric field of the signal beam.

The spectral amplitudes and phases of the TIPTOE data are shown in Fig. 5(b), together with spectrometer data (black line). Overall, a good agreement of both curves is found. The residual differences of the measured spectral amplitudes to the spectrometer data originate in the response function of TIPTOE and in the geometry of the interferometer, see Supplement 1. As apparent from Fig. 5(b), the spectral phase is flat over a broad spectral region but exhibits a curvature at higher frequencies. Its similarity to the expected spectral phase of the materials in the beam path from the fiber exit to the measurement point (black dashed line) confirms that the output phase at the fiber exit is flat. Thus, the presented broadening scheme is in principle self-compressing via means of soliton self-compression (see Supplement 1), where the fiber length aligns with the soliton fission length. The propagation through gas and material introduce a small amount of net dispersion that is responsible for the observation of the faster oscillations after the main pulse, see inset in Fig. 5(a). A polynomial fit yields a residual group delay dispersion of $-3\,\mathrm{fs}^2$ and a third order dispersion of $35\,\mathrm{fs}^3$. Note that in our sign convention, the field at negative times arrives earlier at target than the one at positive times which defines the sign of the curvature of the spectral phase. Those oscillations are only detectable for correct CEP of the pump beam since they originate in the high-frequency part of the spectrum. For the spectral phase of the

Optics EXPRESS

material, we use the refractive index data of Refs. [62–64] for 0.7 m of Neon at 700 mbar, 1 mm of $CaF_2$, and 0.3 mm of fused silica, respectively. We subtract the constant and linear terms to match the phase we found in the experiment. The data of Ref. [62] is only measured in the visible to near-infrared range and is extrapolated to our bandwidth which is a possible explanation for the deviation in the long wavelength range. Additionally, plasma effects on the spectral broadening are found to have minor influence, which is supported by the numerical studies of the fiber dynamics with and without plasma effect (see Supplement 1), but also with overall good agreement of the spectral phase with the material phase in the beam path.

Overall, the multi-octave bandwidth allows for an in-situ CEP calibration due to the observed modulations in the $2f$ region. Even though the response phase of TIPTOE has been discussed and observed before [56,57,59], an investigation of the modulations of the $2f$ components has hitherto been hindered by too narrow band laser sources and therefore required the generation of a second harmonic [54]. With our light source, however, we intrinsically cover that region and can thus calibrate the CEP without any other calibration setups. Intensities in the range of $10^{17}$ W/cm$^2$ are achievable with our system which may drive future strong field experiments even in the relativistic region, at a multi-kilohertz repetition rate.

## 5. Conclusion

We have demonstrated a high-power short-wave infrared spectral broadening scheme providing CEP stability, multi-millijoule pulse energy and high average power. The actual electric field waveform has been successfully characterized with TIPTOE and due to the two octave bandwidth, an in-situ CEP calibration was possible. The self-compressing properties of the fiber eliminate the necessity of post-compression via dispersive mirrors which are prone to transient nonlinearities even at moderate laser intensities that degrade the beam properties [65]. Additionally, the bandwidth limitations of dispersive mirrors can only be overcome by complex light-field synthesis setups [66–68] which our approach eliminates, resulting in a comparatively simple and robust pulse compression scheme. Our approach bypasses constraints for the polarization that are typically caused by dispersive mirrors and thus allows for spectral broadening of arbitrary polarization states. Even though there are new approaches with polarization independent chirped mirrors [69], the supported bandwidth is typically narrower than what is achievable with a self-compression approach as described in this article. We also demonstrated that a static pressure can be used in the fiber and since the window material dispersion and the dispersion in gases counteract each other, a small amount of material can be placed without significant performance degradation. Thus, the compression scheme is appealing to applications outside a vacuum environment.

**Funding.** Max Planck School of Photonics (JB); Laserlab-Europe (871124, MFK); US Department of Energy, Office of Science, Basic Energy Sciences, Scientific User Facilities Division (contract no. DE-AC02-76SF00515 (MFK)); US Department of Energy, Office of Science, Basic Energy Sciences, Chemical Sciences, Geosciences, and Biosciences (CSGB) Division (MFK); Max-Planck-Gesellschaft (Max-Planck Fellowship (MFK)).

**Acknowledgment.** We are grateful for support by Ferenc Krausz providing suitable laboratories. We acknowledge fruitful discussions with Vladislav Yakovlev. We appreciate the technical support by the MPQ technicians as well as by Michael Rogg and his team. A.A. is grateful for the support provided by the Researchers Supporting Project number (RSP2025R152), King Saud University, Riyadh, Saudi Arabia.

**Disclosures.** The authors declare no conflicts of interest.

**Data availability.** Data underlying the results presented in this paper are not publicly available at this time but may be obtained from the authors upon reasonable request.

**Supplemental document.** See Supplement 1 for supporting content.

Optics EXPRESS

## References


1. K. Sugioka and Y. Cheng, "Ultrafast lasers—reliable tools for advanced materials processing," Light: Sci. Appl. **3**(4), e149 (2014).
2. M. Malinauskas, A. Žukauskas, S. Hasegawa, *et al.*, "Ultrafast laser processing of materials: from science to industry," Light: Sci. Appl. **5**(8), e16133 (2016).
3. M. F. Kling, C. S. Menoni, C. Geddes, *et al.*, "Roadmap on basic research needs for laser technology," J. Opt. **27**(1), 013002 (2025).
4. Z. Chang, L. Fang, V. Fedorov, *et al.*, "Intense infrared lasers for strong-field science," Adv. Opt. Photonics **14**(4), 652–782 (2022).
5. F. Krausz and M. Ivanov, "Attosecond physics," Rev. Mod. Phys. **81**(1), 163–234 (2009).
6. M. Nisoli, S. D. Silvestri, O. Svelto, *et al.*, "Compression of high-energy laser pulses below 5 fs," Opt. Lett. **22**(8), 522–524 (1997).
7. T. Nagy, P. Simon, and L. Veisz, "High-energy few-cycle pulses: post-compression techniques," Adv. Phys.: X **6**, 1845795 (2020).
8. M. Nisoli, "Hollow fiber compression technique: A historical perspective," IEEE J. Sel. Top. Quantum Electron. **30**(6: Advances and Applications), 1–14 (2024).
9. R. Szipöcs, K. Ferencz, C. Spielmann, *et al.*, "Chirped multilayer coatings for broadband dispersion control in femtosecond lasers," Opt. Lett. **19**(3), 201–203 (1994).
10. R. Szipőcs and A. Kőházi-Kis, "Theory and design of chirped dielectric laser mirrors," Appl. Phys. B **65**(2), 115–135 (1997).
11. N. L. Wagner, E. A. Gibson, T. Popmintchev, *et al.*, "Self-compression of ultrashort pulses through ionization-induced spatiotemporal reshaping," Phys. Rev. Lett. **93**(17), 173902 (2004).
12. C. Brahms, F. Belli, and J. C. Travers, "Infrared attosecond field transients and uv to ir few-femtosecond pulses generated by high-energy soliton self-compression," Phys. Rev. Res. **2**(4), 043037 (2020).
13. A. Blanco-Redondo, C. M. de Sterke, C. Xu, *et al.*, "The bright prospects of optical solitons after 50 years," Nat. Photonics **17**(11), 937–942 (2023).
14. J. C. Travers, T. F. Grigorova, C. Brahms, *et al.*, "High-energy pulse self-compression and ultraviolet generation through soliton dynamics in hollow capillary fibres," Nat. Photonics **13**(8), 547–554 (2019).
15. J. C. Travers, "Optical solitons in hollow-core fibres," Opt. Commun. **555**, 130191 (2024).
16. C. Brahms and J. C. Travers, "Hisol: High-energy soliton dynamics enable ultrafast far-ultraviolet laser sources," APL Photonics **9**(5), 050901 (2024).
17. F. Köttig, D. Novoa, F. Tani, *et al.*, "Mid-infrared dispersive wave generation in gas-filled photonic crystal fibre by transient ionization-driven changes in dispersion," Nat. Commun. **8**(1), 813 (2017).
18. T. Nagy, M. Forster, and P. Simon, "Flexible hollow fiber for pulse compressors," Appl. Opt. **47**(18), 3264–3268 (2008).
19. P. S. J. Russell, P. Hölzer, W. Chang, *et al.*, "Hollow-core photonic crystal fibres for gas-based nonlinear optics," Nat. Photonics **8**(4), 278–286 (2014).
20. C. Markos, J. C. Travers, A. Abdolvand, *et al.*, "Hybrid photonic-crystal fiber," Rev. Mod. Phys. **89**(4), 045003 (2017).
21. T. Balciunas, C. Fourcade-Dutin, G. Fan, *et al.*, "A strong-field driver in the single-cycle regime based on self-compression in a kagome fibre," Nat. Commun. **6**(1), 6117 (2015).
22. U. Elu, M. Baudisch, H. Pires, *et al.*, "High average power and single-cycle pulses from a mid-ir optical parametric chirped pulse amplifier," Optica **4**(9), 1024–1029 (2017).
23. I. V. Savitsky, E. A. Stepanov, A. A. Lanin, *et al.*, "Single-cycle, multigigawatt carrier–envelope-phase-tailored near-to-mid-infrared driver for strong-field nonlinear optics," ACS Photonics **9**(5), 1679–1690 (2022).
24. C. Vozzi, M. Nisoli, G. Sansone, *et al.*, "Optimal spectral broadening in hollow-fiber compressor systems," Appl. Phys. B **80**(3), 285–289 (2005).
25. E. Granados, L.-J. Chen, C.-J. Lai, *et al.*, "Wavelength scaling of optimal hollow-core fiber compressors in the single-cycle limit," Opt. Express **20**(8), 9099–9108 (2012).
26. K. S. Zinchenko, F. Ardana-Lamas, V. U. Lanfaloni, *et al.*, "Energy scaling of carrier-envelope-phase-stable sub-two-cycle pulses at 1.76 µm from hollow-core-fiber compression to 1.9 mj," Opt. Express **30**(13), 22376–22387 (2022).
27. A. A. Voronin and A. M. Zheltikov, "Subcycle solitonic breathers," Phys. Rev. A **90**(4), 043807 (2014).
28. R.-R. Zhao, D. Wang, Y. Zhao, *et al.*, "Self-compression of 1.8-µm pulses in gas-filled hollow-core fibers*," Chin. Phys. B **26**(10), 104206 (2017).
29. M. F. Seeger, D. Kammerer, J. Blöchl, *et al.*, "49 w carrier-envelope-phase-stable few-cycle 2.1µm opcpa at 10 khz," Opt. Express **31**(15), 24821–24834 (2023).
30. S. Sederberg, F. Kong, and P. B. Corkum, "Tesla-scale terahertz magnetic impulses," Phys. Rev. X **10**(1), 011063 (2020).
31. A. de las Heras, F. P. Bonafé, C. Hernández-García, *et al.*, "Tunable tesla-scale magnetic attosecond pulses through ring-current gating," J. Phys. Chem. Lett. **14**(49), 11160–11167 (2023).
32. K.-H. Hong, C.-J. Lai, J. P. Siqueira, *et al.*, "Multi-mj, khz, 2.1 µm optical parametric chirped-pulse amplifier and high-flux soft x-ray high-harmonic generation," Opt. Lett. **39**(11), 3145–3148 (2014).

Optics EXPRESS


33. Y. Yin, J. Li, X. Ren, *et al.*, "High-efficiency optical parametric chirped-pulse amplifier in bib3o6 for generation of 3 mj, two-cycle, carrier-envelope-phase-stable pulses at 1.7 μm," Opt. Lett. **41**(6), 1142–1145 (2016).
34. Y. Deng, A. Schwarz, H. Fattahi, *et al.*, "Carrier-envelope-phase-stable, 1.2 mj, 1.5 cycle laser pulses at 2.1 μm," Opt. Lett. **37**(23), 4973–4975 (2012).
35. T. Feng, A. Heilmann, M. Bock, *et al.*, "27 w 2.1 μm opcpa system for coherent soft x-ray generation operating at 10 khz," Opt. Express **28**(6), 8724–8733 (2020).
36. J. H. Buss, S. Starosielec, M. Schulz, *et al.*, "Mid-infrared optical parametric chirped-pulse amplifier at 50 w and 38 fs pumped by a high-power yb-innoslab platform," Opt. Express **32**(21), 36185–36192 (2024).
37. S. Reiger, M. Mamaikin, D. Kormin, *et al.*, "Ultra-phase-stable infrared light source at the watt level," Opt. Lett. **49**(4), 1049–1052 (2024).
38. D. Walke, A. Koç, F. Gores, *et al.*, "High-average-power, few-cycle, 2.1 μm opcpa laser driver for soft-x-ray high-harmonic generation," Opt. Express **33**(5), 10006–10019 (2025).
39. M. K. R. Windeler, K. Mecseki, A. Miahnahri, *et al.*, "100 w high-repetition-rate near-infrared optical parametric chirped pulse amplifier," Opt. Lett. **44**(17), 4287–4290 (2019).
40. Y. Shamir, J. Rothhardt, S. Hädrich, *et al.*, "High-average-power 2 μm few-cycle optical parametric chirped pulse amplifier at 100 khz repetition rate," Opt. Lett. **40**(23), 5546–5549 (2015).
41. M. Neuhaus, H. Fuest, M. Seeger, *et al.*, "10 w cep-stable few-cycle source at 2 μm with 100 khz repetition rate," Opt. Express **26**(13), 16074–16085 (2018).
42. Z. Wang, T. Heuermann, M. Gebhardt, *et al.*, "Nonlinear pulse compression to sub-two-cycle, 1.3 mj pulses at 1.9 $\mu$m wavelength with 132 w average power," Opt. Lett. **48**(10), 2647–2650 (2023).
43. L. Eisenbach, Z. Wang, J. Schulte, *et al.*, "Highly efficient nonlinear compression of mj pulses at 2 μm wavelength to 20 fs in a gas-filled multi-pass cell," J. Phys. Photonics **6**(3), 035015 (2024).
44. B. E. Schmidt, A. D. Shiner, P. Lassonde, *et al.*, "Cep stable 1.6 cycle laser pulses at 1.8 $\mu$m," Opt. Express **19**(7), 6858–6864 (2011).
45. S. L. Cousin, F. Silva, S. Teichmann, *et al.*, "High-flux table-top soft x-ray source driven by sub-2-cycle, cep stable, 1.85-$\mu$m 1-khz pulses for carbon k-edge spectroscopy," Opt. Lett. **39**(18), 5383–5386 (2014).
46. T. Nagy, L. von Grafenstein, D. Ueberschaer, *et al.*, "Femtosecond multi-10-mj pulses at 2 μm wavelength by compression in a hollow-core fiber," Opt. Lett. **46**(13), 3033–3036 (2021).
47. D. R. Austin, T. Witting, S. J. Weber, *et al.*, "Spatio-temporal characterization of intense few-cycle 2 μm pulses," Opt. Express **24**(21), 24786–24798 (2016).
48. C. Li, D. Wang, L. Song, *et al.*, "Generation of carrier-envelope phase stabilized intense 1.5 cycle pulses at 1.75 $\mu$m," Opt. Express **19**(7), 6783–6789 (2011).
49. X. Gu, G. Marcus, Y. Deng, *et al.*, "Generation of carrier-envelope-phase-stable 2-cycle 740-$\mu$j pulses at 2.1-$\mu$m carrier wavelength," Opt. Express **17**(1), 62–69 (2009).
50. G. M. Rossi, R. E. Mainz, Y. Yang, *et al.*, "Sub-cycle millijoule-level parametric waveform synthesizer for attosecond science," Nat. Photonics **14**(10), 629–635 (2020).
51. A. Petrulenas, P. Mackonis, and A. M. Rodin, "High-efficiency bismuth borate-based optical parametric chirped pulse amplifier with approximately 2.1 mj, 38 fs output pulses at approximately 2150 nm," High Power Laser Sci. Eng. **11**, e27 (2023).
52. D. Kane and R. Trebino, "Characterization of arbitrary femtosecond pulses using frequency-resolved optical gating," IEEE J. Quantum Electron. **29**(2), 571–579 (1993).
53. R. Trebino and D. J. Kane, "Using phase retrieval to measure the intensity and phase of ultrashort pulses: frequency-resolved optical gating," J. Opt. Soc. Am. A **10**(5), 1101–1111 (1993).
54. S. B. Park, K. Kim, W. Cho, *et al.*, "Direct sampling of a light wave in air," Optica **5**(4), 402–408 (2018).
55. W. Cho, S. I. Hwang, C. H. Nam, *et al.*, "Temporal characterization of femtosecond laser pulses using tunneling ionization in the uv, visible, and mid-ir ranges," Sci. Rep. **9**(1), 16067 (2019).
56. Y. Liu, S. Gholam-Mirzaei, J. E. Beetar, *et al.*, "All-optical sampling of few-cycle infrared pulses using tunneling in a solid," Photonics Res. **9**(6), 929–936 (2021).
57. M. R. Bionta, F. Ritzkowsky, M. Turchetti, *et al.*, "On-chip sampling of optical fields with attosecond resolution," Nat. Photonics **15**(6), 456–460 (2021).
58. Y. Liu, J. E. Beetar, J. Nesper, *et al.*, "Single-shot measurement of few-cycle optical waveforms on a chip," Nat. Photonics **16**(2), 109–112 (2022).
59. J. Blöchl, J. Schötz, A. Maliakkal, *et al.*, "Spatiotemporal sampling of near-petahertz vortex fields," Optica **9**(7), 755–761 (2022).
60. C. Brahms and J. C. Travers, "Luna.jl," (2023).
61. Value provided by the supplier upon request.
62. A. Börzsönyi, Z. Heiner, M. P. Kalashnikov, *et al.*, "Dispersion measurement of inert gases and gas mixtures at 800 nm," Appl. Opt. **47**(27), 4856–4863 (2008).
63. H. H. Li, "Refractive index of alkaline earth halides and its wavelength and temperature derivatives," J. Phys. Chem. Ref. Data **9**(1), 161–290 (1980).
64. I. H. Malitson, "Interspecimen comparison of the refractive index of fused silica*,†," J. Opt. Soc. Am. **55**(10), 1205–1209 (1965).

Optics EXPRESS

65. G. Gui, A. Adak, M. Dandapat, *et al.*, "Measurement and control of optical nonlinearities in dispersive dielectric multilayers," Opt. Express **29**(4), 4947–4957 (2021).
66. A. Wirth, M. T. Hassan, I. Grguraš, *et al.*, "Synthesized light transients," Science **334**(6053), 195–200 (2011).
67. A. Alismail, H. Wang, G. Barbiero, *et al.*, "Multi-octave, cep-stable source for high-energy field synthesis," Sci. Adv. **6**(7), eaax3408 (2020).
68. Z. Pi, H. Y. Kim, and E. Goulielmakis, "Synthesis of single-cycle pulses based on a yb:kgw laser amplifier," Optica **12**(3), 296–301 (2025).
69. Y. Chen, W. Li, Z. Wang, *et al.*, "Complementary dispersive mirror pair produced in one coating run based on desired non-uniformity," Opt. Express **30**(18), 32074–32083 (2022).